Hypoxia-inducible factor-1 drives annexin A2 system-mediated perivascular fibrin clearance in oxygen-induced retinopathy in mice

Bihui Huang,[1,2] Arun B. Deora,[1] Kai-Li He,[1] Kang Chen,[3] Guangzhi Sui,[1] Andrew T. Jacovina,[1] Dena Almeida,[1] Peng Hong,[4] Paul Burgman,[5] and Katherine A. Hajjar[1,2]

[1]Department of Cell and Developmental Biology, Weill Cornell Medical College, New York, NY; [2]Program in Cell and Developmental Biology, Weill Cornell Graduate School of Medical Sciences, New York, NY; [3]Immunology Institute, Department of Medicine, Mount Sinai School of Medicine, New York, NY; [4]Department of Cell Biology, State University of New York Downstate Medical Center, Brooklyn, NY; and [5]Department of Medical Physics, Memorial Sloan-Kettering Cancer Center, New York, NY

Oxygen-induced retinopathy (OIR) is a well-characterized model for retinopathy of prematurity, a disorder that results from rapid microvascular proliferation after exposure of the retina to high oxygen levels. Here, we report that the proliferative phase of OIR requires transcriptional induction of the annexin A2 (A2) gene through the direct action of the hypoxia-inducible factor-1 complex. We show, in addition, that A2 stabilizes its binding partner, p11, and promotes OIR-related angiogenesis by enabling clearance of perivascular fibrin. Adenoviral-mediated restoration of A2 expression restores neovascularization in the oxygen-primed Anxa2$^{-/-}$ retina and reinstates plasmin generation and directed migration in cultured Anxa2$^{-/-}$ endothelial cells. Systemic depletion of fibrin repairs the neovascular response to high oxygen treatment in the Anxa2$^{-/-}$ retina, whereas inhibition of plasminogen activation dampens angiogenesis under the same conditions. These findings show that the A2 system enables retinal neoangiogenesis in OIR by enhancing perivascular activation of plasmin and remodeling of fibrin. These data suggest new potential approaches to retinal angiogenic disorders on the basis of modulation of perivascular fibrinolysis. (*Blood*. 2011;118(10): 2918-2929)

Introduction

Retinopathy of prematurity (ROP) is the main cause of severe visual impairment in children in the developed world.[1] A vascular proliferative disorder that affects preterm and low-birth weight infants on exposure to supraphysiologic oxygen tension, ROP is increasing in incidence with the greater availability of neonatal intensive care, and more frequent survival of very-low-birth weight infants. In the initial, vaso-obliterative phase of ROP, high oxygen exposure provokes endothelial cell death because of oxidative injury, nitrative stress, and suppression of oxygen-related growth factors.[2] In the second phase, the resulting retinal ischemia leads to neovascularization characterized by excessive proliferation and vitreal invasion of blood vessels. This pathologic response arises when neurons and supporting astrocytes become severely metabolically deprived because of vaso-obliteration and produce exaggerated amounts of oxygen-regulated angiogenic factors, such as VEGF and erythropoietin. These agents stimulate the regrowth of abnormal vessels that proliferate toward the vitreous, can form a fibrous scar, and, on contraction, can apply tractional forces that ultimately may detach the retina from its underlying pigment epithelium. Scarring and retinal detachment can lead to vision loss and blindness. Current preventive measures for ROP include restriction of tissue oxygenation and the use of antioxidants, whereas standard treatment for established disease requires ablative laser photocoagulation or cryotherapy. Newer therapies with VEGF-neutralizing antibodies appear promising, but their effects on retinal ganglion cell integrity, the developing cerebral vasculature, and long-term visual acuity and visual fields are unknown.[2]

Annexin A2 is a cell surface phospholipid-binding protein that forms a heterotetrameric complex with its partner S100A10 (p11).[3-5] The receptor complex binds both plasminogen, the precursor of the main fibrinolytic protease, plasmin, and its activator, tissue plasminogen activator (tPA), thereby accelerating the generation of plasmin.[6-8] Mice deficient in annexin A2 (*Anxa2*$^{-/-}$), which also lack normal levels of endothelial cell p11,[9] display fibrin accumulation within microvessels, and their isolated endothelial cells are unable to support tPA-dependent plasminogen activation in vitro.[10] Although they sustain normal spontaneous angiogenesis in embryonic life, *Anxa2*$^{-/-}$ mice exhibit reduced angiogenesis in growth factor–stimulated assays in adulthood. These findings are recapitulated in adult hyperhomocysteinemic mice, in which the A2 protein becomes derivatized by disulfide linkage with homocysteine, thus preventing tPA binding and plasmin generation.[11]

Here, we examined the A2 system in oxygen-induced retinopathy (OIR), a model of pathologic, hypoxia-driven angiogenesis. We found that hypoxia induces the expression of A2 through direct transcriptional induction by hypoxia-inducible factor-1 (HIF-1). A2 enabled retinal neovascularization, and the angiogenic block observed in the *Anxa2*$^{-/-}$ retina reflected impairment of cell surface fibrinolysis and reduced cell migration in a fibrin-rich milieu. We demonstrated that depletion of fibrinogen exaggerates, while inhibition of plasminogen activation attenuates, oxygen-induced neoangiogenesis in the retina. Our findings highlight the importance of A2-related fibrinolysis in oxygen-induced neoangiogenesis and could serve as the basis for targeting the A2 system as a

Submitted March 5, 2011; accepted June 30, 2011. Prepublished online as *Blood* First Edition paper, July 15, 2011; DOI 10.1182/blood-2011-03-341214.

The online version of this article contains a data supplement.

The publication costs of this article were defrayed in part by page charge payment. Therefore, and solely to indicate this fact, this article is hereby marked "advertisement" in accordance with 18 USC section 1734.

potentially novel therapeutic intervention for ROP and other proliferative retinal vascular disorders.

Methods

Mice

Anxa2$^{+/+}$ and *Anxa2*$^{-/-}$ mice were generated on the C57Bl/6 background as previously described.[10] These mice were intercrossed for ≥ 10 generations with wild-type 129/SVJ mice to generate both genotypes on the 129/SVJ background. *Anxa2*$^{+/+}$ and *Anxa2*$^{-/-}$ mice exhibited no significant differences in body mass in the course of the experiments. All animal procedures were approved by the Institutional Animal Care and Use Committee of Weill Cornell Medical College.

Oxygen-induced retinopathy

OIR was induced as previously described with the use of a BioSpherix ProOX A chamber equipped with ProOx P110 single set point oxygen controller, E702 oxygen sensor, and ProCo2 carbon dioxide sensor. Postnatal day 7 (P7) mouse pups together with their dam were placed for 5 consecutive days (P7-P12) in a chamber in which the ambient oxygen level was maintained at 75% ± 2%. On P12, they were returned to room air (21% O_2). Control pups were maintained in room air throughout the experiment.[12] Mouse retinas were isolated and assayed by immunoblot, RT-PCR, quantitative RT-PCR, immunostaining, and ELISA on days 2-6 after hyperoxia (P14-P18).

Retinal whole mounts

Eyes from P17 *Anxa2*$^{+/+}$ and *Anxa2*$^{-/-}$ mice subjected to room air (21% O_2) or hyperoxia (75% O_2) were enucleated, and retinas were harvested for analysis by whole mount assay as described.[13] Areas of retinal vaso-obliteration and neovascularization from both *Anxa2*$^{+/+}$ and *Anxa2*$^{-/-}$ mice were quantified according to Connor et al.[14] Whole mount retinal images (Figures 1B, 2B, 6D, and 7D) were acquired at room temperature using a Micromax Camera (ST133; Princeton Instruments Inc) equipped with Metamorph 7.7 software, and coupled to a fluorescence scanning microscope (Axiovert 200M; Zeiss) equipped with a 5×/0.15 plan-neofluar objective lens; images were further processed using PhotoShop 7.0.

Cryosection preparation

Under general anesthesia, P17 mice were perfused intracardially with cold PBS containing 5 U/μL heparin sodium (Sigma-Aldrich) at 80 cm H_2O pressure (10 minutes) as described.[10] The mouse eyes were collected and fixed in 2% paraformaldehyde after creating a nick in the anterior cornea. The lenses were removed, and the remaining tissues were cryoprotected in 30% sucrose in PBS (24 hours) and then transferred to cryosection buffer (30% sucrose: OCT = 1:2; 4°C) for infiltration. The samples were transferred to foil molds filled with cryosection buffer, oriented with the optical nerve facing up, frozen in 2-methylbutane, chilled in liquid nitrogen, and stored at −80°C before sectioning. Cryosections were prepared by cutting the embedded tissue along its vertical axis and stored at −20°C before further analysis.

Immunohistochemistry

Cryosections were air dried at 21°C for 30 minutes and then refixed with ice-cold acetone (10 minutes). After 3 washes with PBS, the sections were boiled in antigen retrieval buffer (0.01M sodium citrate, pH 6.0; 20 minutes) with the use of Antigen Retriever (PickCell Laboratories) and then processed for staining with the use of monoclonal anti-A2 IgG (Zymed) and the MOM kit (Vector Laboratories) according to the manufacturer's instructions. For fibrin staining, cryosections were incubated with rabbit IgG directed against fibrinogen (2 hours, 21°C; Dako) and then incubated with Cy3-conjugated donkey anti–rabbit IgG (30 minutes, 21°C; Jackson Immunoresearch Laboratories). Finally, the sections were counterstained with fluorescein-conjugated isolectin B4 and 4′-6′-diamidine-2-phenylindole (DAPI; Invitrogen). Antibodies for immunohistochemistry are listed in supplemental Table 2 (available on the *Blood* Web site; see the Supplemental Materials link at the top of the online article). After staining, images of retinal sections (Figures 1D, 2D, 3C, 5A,C, 6B, and 7B) were acquired at room temperature using a Retiga camera (1300i, QImaging) equipped with Qcapture 2.98.2 software, and coupled to a fluorescence microscope (Eclipse 80i, Nikon) equipped with either a 4×/0.2 or 20×/0.75 plan Apo objective lens; images were further processed using Photoshop 7.0.

Tuft counting

Retinal cryosections were stained with fluorescein-conjugated isolectin B4 and DAPI as described. Neovascular nuclei within isolectin-positive cells were enumerated under fluorescence microscopy (magnification ×200, merge filter; Nikon 80i).

Cell culture

Anxa2$^{+/+}$ and *Anxa2*$^{-/-}$ mouse cardiac microvascular endothelial cells (CMECs) were isolated and evaluated in migration assays as previously described.[10] HUVECs were isolated and propagated in M199 Medium (Invitrogen) supplemented with 20% FBS (Invitrogen), 20 μg/mL endothelial cell growth supplement (Sigma-Aldrich), 100 μg/mL heparin (Sigma-Aldrich), 2mM L-glutamine, 100 U/mL penicillin G, and 0.1 mg/mL streptomycin sulfate at 37°C in a 5% CO_2 atmosphere, as previously described.[15] *Hif1a*$^{+/+}$ and *Hif1a*$^{-/-}$ mouse embryonic fibroblasts[16] (courtesy of Dr Gregg Semenza, Johns Hopkins University School of Medicine), HEK 293 and HEK 293AD cells (Stratagene) were cultured in DMEM (Invitrogen) supplemented with 10% FBS, 2mM L-glutamine, 100 U/mL penicillin G, and 0.1 mg/mL streptomycin sulfate at 37°C in 5% CO_2.

Nuclear and cytoplasmic protein extraction

Nuclear protein was isolated from cultured cells and retinas with the use of an extraction kit (NE-PER Nuclear and Cytoplasmic Extraction Kit; Thermo Scientific) according to the manufacturer's instructions. Cytoplasmic retinal proteins were extracted as described[15] with the use of 3 repetitions of 6-second sonication pulses (30% maximum output) on ice with a Branson Sonifier (VWR). Protein concentration was estimated using the BCA reagent (Thermo Scientific).

Immunoblotting

Proteins extracted from cultured cells and harvested retinas were resolved on 10% or 15% SDS-polyacrylamide gels and transferred to nitrocellulose membranes (Bio-Rad). The blots were probed with mouse IgG directed against A2, human p11, HIF-1α (all from BD Transduction Labs); HIF-1β (Novus); Erk1/2, Tyr 416 phospho-Src, Src (all from Cell Signaling Technology); and fibrinogen (Dako; supplemental Table 2). For detection of mouse p11, a peptide representing a portion of the mouse p11 protein (CGDKDHLTKEDLRVLMERE) was conjugated to keyhole limpet hemocyanin and used to immunize rabbits (Covance Research Products Inc); IgG was purified from antisera by protein G affinity. α-actin (Santa Cruz Biotechnology), and pan-cadherin (Cell Signaling Technology) served as cytoplasmic and cell surface protein-loading controls, respectively.[10,15] Fibrin immunoblotting of mouse retinas was performed as described.[10] Immunoblots were incubated with secondary antibodies, conjugated to horseradish peroxidase, and directed against mouse or rabbit IgG. Immunoreactivity was visualized by chemiluminescence (ECL or ECL plus; GE Healthcare) and quantified by Scion Image.

Quantitative RT-PCR

Total RNA was extracted from cultured cells and retinas with the use of Trizol (Invitrogen) according to manufacturer's protocol. The concentration and purity of RNA were estimated by measuring OD260/280. mRNA levels of A2, p11, VE-cadherin 5, and HIF-1α were assessed with a one-step RT-PCR kit (QIAGEN) according to the manufacturer's instructions. GAPDH or β-actin was used as a loading control. Primers used for RT-PCR

are listed in supplemental Table 1. For quantitative RT-PCR, mRNA was converted to cDNA by reverse transcription (QIAGEN). Equal quantities of cDNA were subjected to real-time PCR with the use of the Sybr-green real-time PCR kit (Applied Biosystems). Each sample was run in duplicate. The results were expressed as the mean relative expression compared with control samples. The primers (RealTimePrimers.com) used are listed in supplemental Table 1.

Recombinant adenovirus construction and infection

A recombinant adenovirus encoding either A2 or p11 was constructed with the pAdEasy system.[17] With the use of the following primers: 5′-CTCTCTCGGTACCCTTCAAAATGTCTACTGTCCACG-3′ (sense) and 5′-CTACTCTTCTAGATCAGTCATCCCCACCACACAGGTAC-3′ (antisense) for *Anxa2* and 5′-CTCTCTCAAGCTTCTTCAAAATGCCATC-CCAAATGG-3′ (sense) and 5′-TGTGCTGTCTAGACTATTTCTTC-CCCTTCTGCTTC-3′ (antisense) for *S100a10*, A2 or p11 cDNAs were amplified and subcloned into a shuttle vector containing a green fluorescent protein reporter gene, pAdTrack-CMV. This plasmid was recombined with pAdEasy-1, the replication-deficient adenovirus backbone. The recombinant adenovirus encoding A2 or p11 was allowed to proliferate and then was packaged in HEK 293 cells and purified by CsCl gradient ultracentrifugation. The shuttle vector (pAdTrack-CMV) and replication-deficient adenovirus backbone (pAdEasy-1) were kindly provided by Dr Bert Vogelstein (John Hopkins University School of Medicine). *Anxa2*$^{-/-}$ mouse CMECs were infected with empty, A2-, or p11-encoding recombinant adenoviruses at a concentration of 1000 particles per cell. The efficiency of infection, monitored by fluorescence microscopy, was ~ 60%.

Cell surface protein biotinylation

Analyses of cell surface expression of A2 and p11 were conducted as described.[15] Gel loading was assessed by evaluation of immunoreactivity of IgG directed against pan-cadherin (Cell Signaling Technology).

Immunoprecipitation

Detection of Tyr^{23}-phosphorylated A2 was performed as described with the use of antibodies described in supplemental Table 2.[15]

Plasmin generation assay

tPA-dependent plasmin generation was assayed as previously described.[18]

Cell migration assay

Directed migration of HUVECs and *Anxa2*$^{+/+}$ and *Anxa2*$^{-/-}$ CMECs through fibrin barriers in response to VEGF-A was quantified as described.[10]

Enzyme-linked immunosorbent assay

Plasma fibrinogen, VEGF, and placental growth factor (PlGF) levels in mouse retinas and other organs were estimated with the use of ELISA kits (R&D Systems) according to the manufacturer's instructions.

mRNA stability assay

Stability of A2 mRNA was assessed by pretreating HUVECs with or without actinomycin D (10 μg/mL; 6 hours) before assaying mRNA and protein by RT-PCR and immunoblot analysis.[19]

Electrophoretic mobility shift assay

Interaction between HIF-1 protein and a portion of the human A2 promoter containing a putative hypoxia responsive element (HRE; supplemental Figure 3C) was examined by EMSA as described.[20] Probes for the *ANXA2* gene consisted of 5′-GAGCTCGACGTGGCACTTAAG-3′ (wild type) and 5′-GAGCTCGAAAAAGCACTTAAG-3′ (mutant). Probes for the *VEGFA* gene were 5′-TGCATACGTGGGCTCCAACAG-3′ (wild type) and 5′-TGCATAAAAGGGCTCCAACAG-3′ (mutant).

Chromatin immunoprecipitation

HUVECs were cultured in 150-mm^2 dishes and treated with 200μM $CoCl_2$ or PBS for 16 hours and then were harvested. Interaction between HIF-1α protein and human A2 promoter was tested with the use of the Easy ChIP assay kit (Millipore).[16] Primers for amplification of the human A2 promoter fragment were 5′-CCACTTAATCAAGCCCAGAGTC-3′ (sense) and 5′-CGCCACGCGGGAGCGGCCCCAG-3′ (antisense).

Promoter reporter assay

A 40-bp A2 promoter probe containing either the wild-type (5′-GAGCTCGACGTGGCACTTAAGAGGCTCTGCTCAGCATTTG-3′) or mutant (5′-GAGCTCGAAAAGGCACTTAAGAGGCTCTGCTCAG-CATTTG-3′) HRE was subcloned into the luciferase reporter vector pGL3-luc. The HEK 293 cells, cultured in 48-well dishes, were transfected in triplicate with the use of lipofectamine 2000 (Invitrogen) according to the manufacturer's instructions with a total of 1.5 μg of DNA, consisting of different combinations of plasmids. HIF-1α (pcDNA3.1/*Hif-1a*) and HIF-1β (pBM5/*Hif-1b*) expression vectors, kindly provided by Dr Gregg Semenza (Johns Hopkins University School of Medicine) and Dr Oliver Hankinson (University of California Los Angeles Medical Center), respectively, induced robust protein expression (supplemental Figure 4B). A luciferase reporter vector containing the wild-type VEGF promoter was kindly provided by Dr Lee Ellis (M. D. Anderson Cancer Center). Reporter activity was quantified as luciferase activity (Promega).

Flow cytometry

Surface expression of A2 on HUVECs cultured in 21% or 0.5% O_2 for 16 hours was measured by flow cytometry with the use of either mouse monoclonal IgG1 directed against human/mouse A2 (BD Biosciences), PE-conjugated VE-cadherin 5 (BD PharMingen), or nonimmune monoclonal mouse IgG1 isotype control (R&D Systems; supplemental Table 2). Secondary antibodies consisted of Alexa Fluor 647–conjugated goat anti–mouse IgG (Invitrogen/Molecular Probes). Labeled cells were analyzed with a BD LSR II flow cytometer (BD Biosciences). Nonviable cells were excluded from the analysis with the use of 7-amino-actinomycin D (BD Biosciences).

Ancrod and tranexamic acid treatment

For fibrinogen depletion, ancrod (National Institute for Biological Standards and Control) was administered from P12 to P16 (2 U/d subcutaneously), immediately after transfer of the mice from 75% oxygen to room air. To inhibit plasminogen activation, mice were given tranexamic acid (2.5 mg intraperitoneally every 8 hours; Sigma-Aldrich).

Statistical analysis

Statistical significance was assessed by the 2-tailed Student *t* test. *P* values of ≤ .05 were considered statistically significant.

Results

Annexin A2 promotes oxygen-induced retinal neovascularization

With the use of 2 independent criteria, we quantified retinal neovascularization in P17 *Anxa2*$^{+/+}$ and *Anxa2*$^{-/-}$ neonatal mice subjected to 75% oxygen for 5 days (P7-P12).[13,14] We found no significant difference in the ratio of the area of vaso-obliteration to total retinal area in *Anxa2*$^{+/+}$ (25.6% ± 1.0%) and *Anxa2*$^{-/-}$ (27.5% ± 1.1%) mice ($P = .23$). However, we did detect a 2.5-fold reduction in the ratio of retinal neovascularization to total retinal area in *Anxa2*$^{-/-}$ mice (4.7% ± 0.4%) compared with Anxa2$^{+/+}$ mice (12.1% ± 0.5%; $P = 1.3 \times 10^{-7}$; Figure 1A-C). In addition,

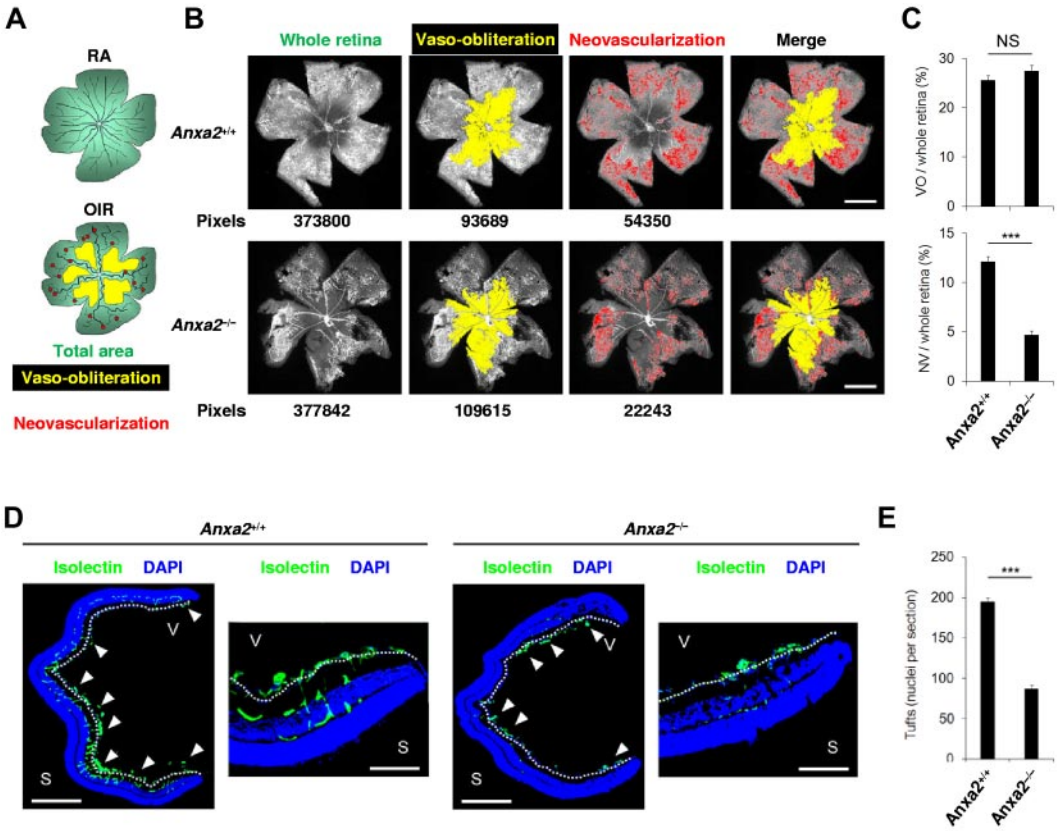

Figure 1. The annexin A2 system promotes retinal neoangiogenesis in OIR. (A) Schematic diagram showing areas occupied by total retina (green), regions of vaso-obliteration (yellow), and regions of neovascularization (red) in mice maintained in room air (RA) or treated with oxygen from P7 to P12 (OIR). (B) Representative retinal images showing total retinal area and regions of vaso-obliteration and neovascularization in P17 oxygen-treated *Anxa2*$^{+/+}$ and *Anxa2*$^{-/-}$ mice. Pixel number corresponding to each compartment is indicated below each image. (C) Ratios of vaso-obliterative (VO) to total retinal area (25.6% ± 1.0% vs 27.5% ± 1.1%) and neovascular (NV) to total retinal area (12.1% ± 0.5% vs 4.7% ± 0.4%) in oxygen-treated P17 *Anxa2*$^{+/+}$ (n = 7) and *Anxa2*$^{-/-}$ (n = 9) mice (NS indicates no significant difference; ***$P < .001$). (D) Representative retinal cross-sections (magnification ×40), with close-up views of peripheral region (magnification ×200) of retinas from oxygen-treated P17 *Anxa2*$^{+/+}$ and *Anxa2*$^{-/-}$ mice stained with DAPI (blue) and isolectin B4 (green). Neovascular tufts penetrating the inner limiting membrane (highlighted with a white dashed line) are indicated by arrowheads. (E) Enumeration of neovascular nuclei in retinal sections from P17 oxygen-treated Anxa2$^{+/+}$ versus Anxa2$^{-/-}$ (194.5 ± 5.2; n = 8 vs 87.4 ± 4.6; n = 10; ***$P < .001$) mice. Scale bars, 200 μm (B; magnification ×50), 500 μm (D; magnification ×40), 100 μm (D; magnification ×200).

enumeration of neovascular tufts by immunofluorescent isolectin B4 staining of retinal sections (Figure 1D) showed a > 50% reduction in the number of vascular structures extending beyond the internal limiting membrane in *Anxa2*$^{-/-}$ (87.1 ± 4.6) versus *Anxa2*$^{+/+}$ (194.5 ± 5.2) retinas at P17, 5 days after release from hyperoxia ($P = 1.12 \times 10^{-10}$; Figure 1E). No difference was observed in VEGF or PlGF induction in *Anxa2*$^{+/+}$ compared with *Anxa2*$^{-/-}$ mice (supplemental Figure 1A-B), and no difference was observed in neonatal retinal vascularization when *Anxa2*$^{+/+}$ and Anxa2$^{-/-}$ mice were maintained in room air (0-2 tufts per section; supplemental Figure 2).

Subretinal injection of a replication-deficient A2-encoding adenovirus restored A2 expression in *Anxa2*$^{-/-}$ mouse retinas, as shown by RT-PCR and immunoblot analysis of retinal tissue (Figure 2A). At the same time, restoration of A2 expression augmented OIR-related neovascularization (4.7% ± 0.15% vs 8.6% ± 0.12%; $P = 6.4 \times 10^{-5}$) of *Anxa2*$^{-/-}$ retinas without changing the degree of vaso-obliteration (19.5% ± 0.64% vs 19.4% ± 0.79%; $P = .91$; Figure 2B-C). Viral transduction of A2 also increased by 60% the number of neovascular tuft nuclei in *Anxa2*$^{-/-}$ eyes in comparison to contralateral *Anxa2*$^{-/-}$ eyes injected with empty virus (88 ± 4.2 vs 134 ± 3.5; $P = 9.0 \times 10^{-6}$; Figure 2D-E). Together, these data indicate that the complete OIR response depends on the presence of an intact A2 system.

HIF-1 directly regulates annexin A2 gene expression

We determined whether retinal A2 and p11 expression is regulated by oxygen tension. Although p11 mRNA levels remained relatively constant in the retina after high oxygen exposure, A2 mRNA levels increased by 2- to 4-fold at P14-P18 (Figure 3A). Protein levels of both A2 and p11 increased by 2- to 5-fold at P16-P18 in comparison to the corresponding RA value, as shown by immunoblot analysis of retinal lysates (5.4-fold ± 1.2-fold at P16 and 2.0-fold ± 0.2-fold at P18, n = 6, for A2; 4.1-fold ± 0.6-fold at P16 and 2.2-fold ± 0.3-fold at P18, n = 4, for p11, SE; Figure 3B). The increased A2 was further confirmed by immunofluorescence staining of retinal sections (Figure 3C). We showed previously that A2 stabilizes p11 posttranslationally in endothelial cells by masking a polyubiquitination site in the C-terminal region of p11,[9] a finding that explains the increase in p11 protein in the absence of any alteration in p11 mRNA.

To ascertain whether A2 synthesis might be governed by the HIF-1 transcription complex, a master regulator of oxygen-sensitive genes, we first confirmed that HIF-1α was stabilized during OIR. Indeed, from P12 to P18, HIF-1α mRNA did not change (supplemental Figure 3A-B), but protein levels increased 2- to 4-fold in comparison to the corresponding RA value (0.4-fold ± 0.1-fold at P12; 2.3-fold ± 0.3-fold at P14; 4.3-fold ± 0.9-fold at P16; 4.0-fold ± 0.5-fold at P18; n = 3; SE; Figure 3D). In

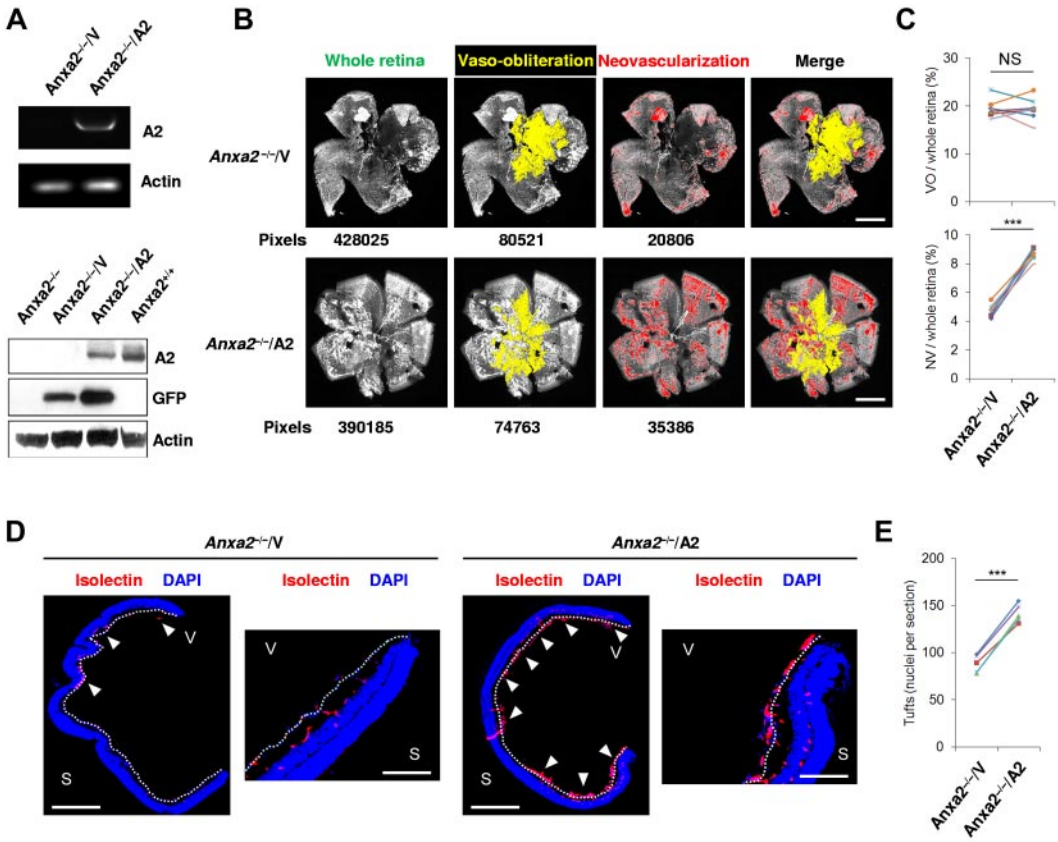

Figure 2. Reexpression of annexin A2 restores neoangiogenesis in OIR. (A) RT-PCR of retinal tissue at P14 after subretinal injection of A2-encoding (A2; OD) or empty (V; OS) adenovirus in Anxa2$^{-/-}$ mice at P12, and immunoblot analysis of identically treated *Anxa2*$^{-/-}$ mouse retinas 2 days (P14) after virus injection. The data are representative of 3 independent experiments. (B) Representative retinal images showing total retinal area and regions of NV and VO in oxygen-treated P17 *Anxa2*$^{-/-}$ mice injected with either A2-encoding or empty virus on P12. Pixel number corresponding to each compartment is indicated below each image. (C) Ratios of VO to total retinal area (19.5% ± 0.64% vs 19.4% ± 0.79%) and NV to total retinal area (4.7% ± 0.15% vs 8.6% ± 0.12%) in P17 oxygen-treated *Anxa2*$^{-/-}$ mice injected with either empty or A2-encoding virus (n = 8; NS indicates no significant difference, ***$P < .001$). (D) Representative retinal cross-sections (magnification ×40), with a close-up view of the peripheral region (magnification ×200) of retinas from P17 oxygen-treated *Anxa2*$^{-/-}$ mice injected with empty or A2-encoding virus stained with DAPI (blue) and isolectin B4 (red). Neovascular tufts penetrating the inner limiting membrane (highlighted with a white dashed line) are indicated by arrowheads. (E) Enumeration of neovascular nuclei in retinal sections from P17 oxygen-treated *Anxa2*$^{-/-}$ mice injected with empty versus A2-encoding virus (88 ± 4.2 vs 134 ± 3.5; n = 5; ***$P < .001$). S indicates sclera; V, vitreous body. Scale bars, 200 μm (B; magnification ×50), 500 μm (D; magnification ×40), 100 μm (D; magnification ×200).

HUVECs treated either with $CoCl_2$, a heavy metal salt that mimics hypoxia,[21] or with hypoxia itself (0.5% O_2), protein levels of HIF-1α (29.4-fold ± 1.3-fold for 0.5% O_2 and 90.6-fold ± 7.0-fold for $CoCl_2$, n = 3), A2 (2.4-fold ± 0.6-fold for 0.5% O_2, n = 6 and 2.6-fold ± 0.5-fold for $CoCl_2$, n = 4), and p11 (2.3-fold ± 0.4-fold, n = 6 for 0.5% O_2 and 2.3-fold ± 0.3-fold for $CoCl_2$, n = 4) all increased (Figure 3E). $CoCl_2$ proved to be an even stronger stimulus than hypoxia for stabilization of HIF-1α; this is most probably because $CoCl_2$ acts by inhibiting the prolyl hydroxylase that allows HIF-1α to be ubiquitinated and destroyed in the proteasome, whereas hypoxia reduces, but does not eliminate, oxygen, a key co-substrate for the hydroxylating enzyme.[22] Elevations in mRNA levels for A2, but not HIF-1α or p11, were observed over the same time frame (Figure 3E).

mRNA stability assays showed that hypoxia-related induction of A2 in HUVECs reflected transcriptional activation. Because A2 was up-regulated in *Hif1a*$^{+/+}$ (2.6-fold ± 0.4-fold for 0.5% O_2 and 2.4-fold ± 0.3-fold for $CoCl_2$, n = 6, SE), but not *Hif1a*$^{-/-}$ (1.0-fold ± 0.1-fold for 0.5% O_2 and 0.9-fold ± 0.1-fold for $CoCl_2$, n = 6, SE), mouse embryonic fibroblasts[16] on treatment with either $CoCl_2$ or hypoxia (Figure 3F), we concluded that its induction depended on HIF-1α. Similarly, p11 was up-regulated in *Hif1a*$^{+/+}$ mouse embryonic fibroblast (MEFs; 2.3-fold ± 0.3-fold for 0.5% O_2 and 2.7-fold ± 0.5-fold for $CoCl_2$, n = 6, SE) but not in *Hif1a*$^{-/-}$ MEFs (1.0-fold ± 0.1-fold for 0.5% O_2 and 1.1-fold ± 0.1-fold for $CoCl_2$, n = 6, SE). Examination of the A2 promoter sequence showed a nearly complete HRE (supplemental Figure 3C). In addition, A2 expression was stable in the presence of actinomycin D, suggesting that increased mRNA levels induced by hypoxia reflected an increased rate of transcription (supplemental Figure 4A). An EMSA[20] showed that A2 probes containing wild-type, but not mutant, HREs from the A2 promoter interacted specifically with nuclear components from HEK 293 cells that overexpressed HIF-1α and HIF-1β (Figure 3G; supplemental Figure 4B). A ChIP assay,[16] furthermore, confirmed direct binding of HIF-1α to the A2 promoter in HUVECs treated with $CoCl_2$ (Figure 3H). A similar A2 promoter sequence was activated by the HIF-1 complex in luciferase assays (Figure 3I). Together these experiments showed that A2 synthesis is regulated by hypoxia at the transcriptional level through the action of HIF-1.

Enhanced annexin A2 expression during hypoxia promotes plasminogen activation and endothelial cell migration

We showed previously that cell surface expression of A2, a Src substrate, depends on both the presence of p11 and phosphorylation of Tyr[23] by active pp60Src kinase.[15] Here, cell surface biotinylation showed a clear increase in endothelial cell surface expression of

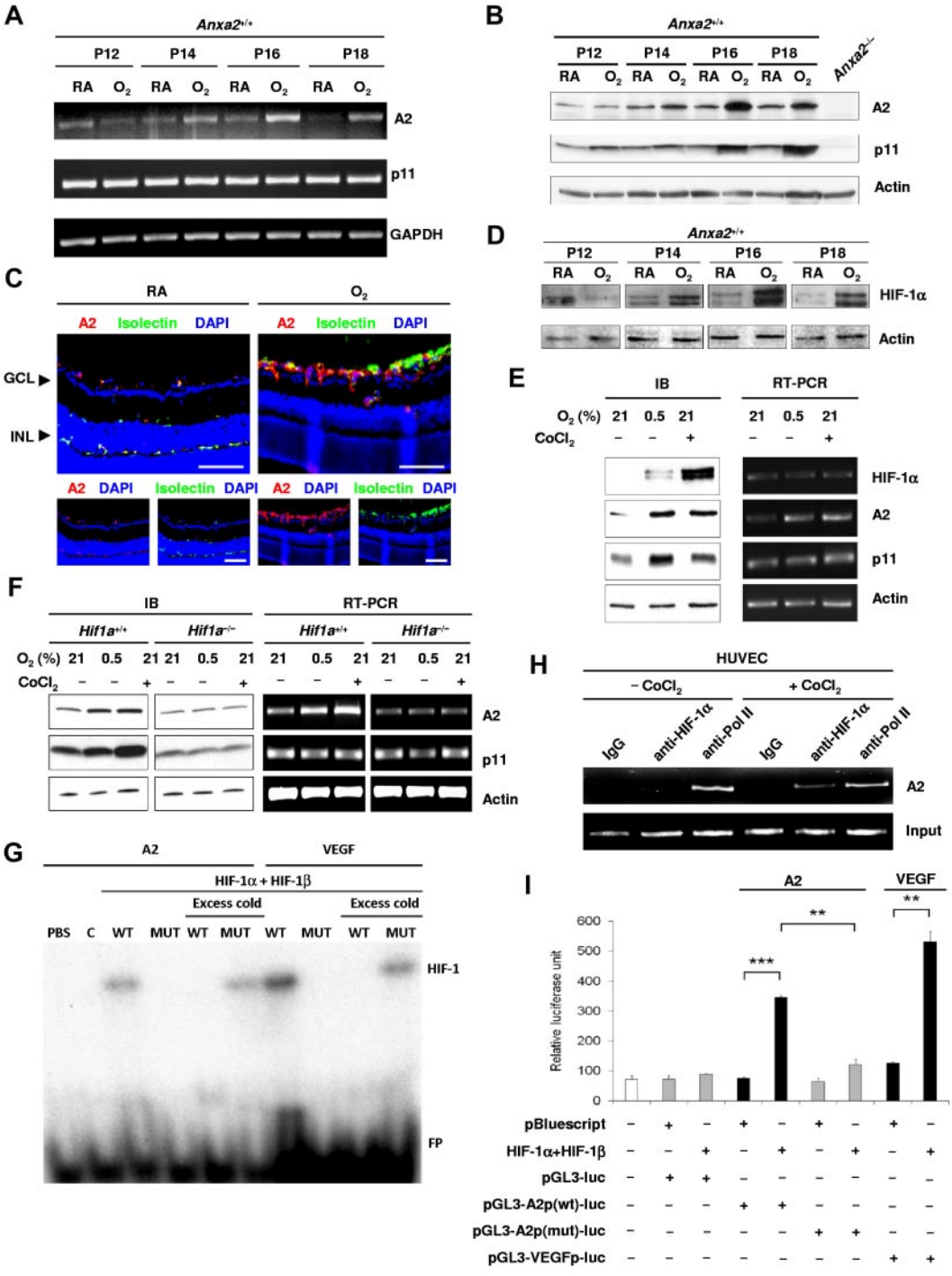

Figure 3. Annexin A2 is up-regulated during hypoxia through Hif-1α–mediated signaling. (A) RT-PCR determination of the fold change in Anxa2 and S100a10 mRNA levels in P12-P18 retinas from *Anxa2*$^{+/+}$ mice after treatment with oxygen. GAPDH mRNA served as a loading control. (B) Representative immunoblot of *Anxa2*$^{+/+}$ retinal A2 and p11 at P12, P14, P16, and P18 after treatment with oxygen (O_2) or room air (RA). Actin was used as loading control. (C) Representative images of retinal sections from P17 *Anxa2*$^{+/+}$ mice either maintained in RA or treated with O_2 and stained with anti-A2 (red), isolectin B4 (green), and DAPI (blue). GCL indicates ganglion cell layer; INL, inner nuclei layer. Scale bars, 75 μm (magnification ×200). (D) Immunoblot of HIF-1α in P12, P14, P16, and P18 retinas from *Anxa2*$^{+/+}$ mice maintained in RA or treated with O_2. Actin served as the loading control. (E) Immunoblot and RT-PCR analyses of HIF-1α, A2, and p11 in HUVECs after treatment with either 0.5% O_2 or 200μM $CoCl_2$ for 16 hours. Actin served as the loading control. (F) Immunoblot and RT-PCR analyses of A2 and p11 in *Hif1a*$^{+/+}$ and *Hif1a* $^{-/-}$ mouse embryonic fibroblasts after treatment with either 0.5% O_2 or 200μM $CoCl_2$ for 16 hours. Actin served as the loading control. (G) EMSA showing interaction between the HIF-1 complex and *ANXA2* or *VEGFA* promoter probes. C indicates control; WT, *ANXA2* or *VEFGA* probe containing wild-type HRE; MUT, *ANXA2* or *VEGFA* probe containing mutant HRE; FP, free unbound probe. (H) ChIP assay showing interaction between HIF-1α and the *ANXA2* promoter. Preimmune IgG and anti-RNA polymerase II served as negative and positive controls, respectively. (I) Luciferase assay showing activation of *ANXA2* and *VEGFA* promoters by HIF-1 complex in HEK 293 cells (n = 3; *$P < .05$, **$P < .01$, and ***$P < .001$). The data are representative of 3 (A, C, D, G, H, and I) and 6 (B, E, and F) separate experiments.

A2, as well as p11, after true hypoxia (Figure 4A). This increase was further quantified by flow cytometry, which showed an increase of 3- to 4-fold (mean fluorescence intensity, 10.4 at 21% O_2 vs 36.1 units in 0.5% O_2; Figure 4B). At the same time, cell

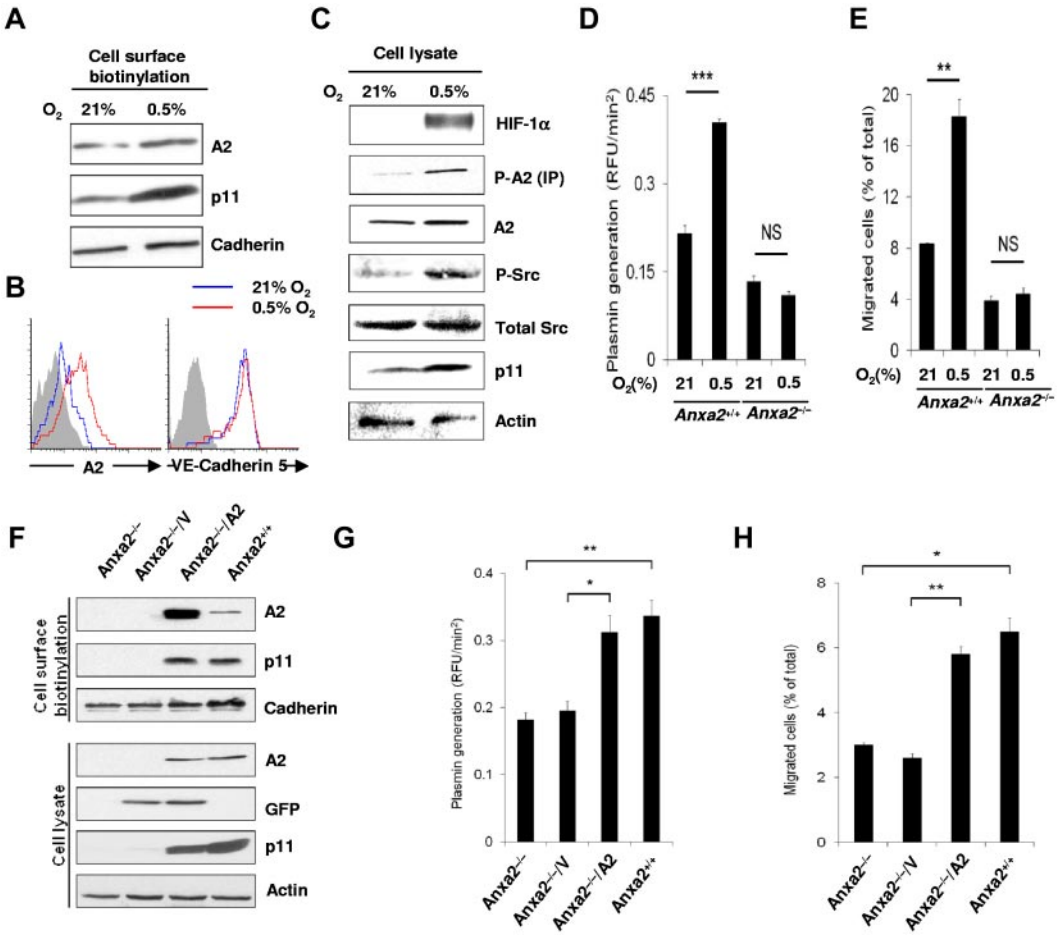

Figure 4. Hypoxia promotes functional endothelial cell surface expression of A2. (A) Immunoblot of cell surface biotinylated A2 and p11 on HUVECs treated with hypoxia (0.5% O_2, 16 hours). Pan-cadherin served as the loading control. (B) Flow cytometric analysis of HUVEC surface A2 and VE-cadherin 5 after normoxia (21% O_2, 16 hours; blue histograms) or hypoxia (0.5% O_2, 16 hours; red histograms). Isotype-matched IgG served as control (shaded histogram). (C) Immunoblot showing total cellular HIF-1α, total A2, Tyr 416 phospho-Src, total Src, p11, and actin after hypoxia (0.5% O_2, 16 hours). Phospho-A2 was captured by immunoprecipitation, followed by immunoblot analysis. (D) $Anxa2^{+/+}$ and $Anxa2^{-/-}$ CMEC-associated plasmin generation for cells maintained in 21% versus 0.5% O_2 (0.22 ± 0.014 vs 0.404 ± 0.005 vs 0.13 ± 0.01 vs 0.11 ± 0.007; n = 6; $^{**}P < .01$; NS indicates no significant difference). (E) Migration of $Anxa2^{+/+}$ (8.35% ± 0.074% vs 18.3% ± 1.36%) and $Anxa2^{-/-}$ (3.9% ± 0.34% vs 4.4% ± 0.5%) CMECs maintained in 21% or 0.5% O_2 (16 hours, n = 3; $^{**}P < .01$). (F) Immunoblot of surface and intracellular A2 and p11 in $Anxa2^{-/-}$ CMECs 48 hours after infection with either empty or A2-encoding viruses. Pan-cadherin and actin served as surface and intracellular protein loading controls, respectively. (G) $Anxa2^{-/-}$ CMEC-associated plasmin generation after infection with empty (V; 0.195 ± 0.014 RFU/min^2) or A2-encoding virus (A2; 0.312 ± 0.025 RFU/min^2; 48 hours, n = 3; $^{*}P < .05$, $^{**}P < .01$). (H) Migration of $Anxa2^{-/-}$ CMECs infected with either empty (V; 2.6% ± 0.14%) or A2-encoding virus (A2; 5.8% ± 0.23%; 48 hours, n = 3; $^{*}P < .05$, $^{**}P < .01$). The data are representative of 3 independent experiments (A-H).

surface VE-cadherin 5 remained constant (mean fluorescence intensity, 171.4 at 21% O_2 vs 169.2 units in 0.5% O_2), indicating the specificity of the A2 response.

Total cellular levels of both Tyr^{23} phosphorylated A2 (phospho-A2) and active Src (Tyr^{416} phosphorylated Src) increased along with HIF-1α and p11 (Figure 4C). We noted that hypoxia-induced increases in both tPA-dependent plasmin generation and cell migration through a fibrin barrier were A2 dependent, being observed in $Anxa2^{+/+}$, but not $Anxa2^{-/-}$, mouse microvascular endothelial cells (Figure 4D-E). Both plasmin generation and cell migration through a fibrin barrier nearly doubled after restoring A2 and p11 expression in $Anxa2^{-/-}$ mouse endothelial cells through transduction with an A2-encoding adenovirus (Figure 4F-H). These data indicate that hypoxia enhances both A2 expression and plasminogen activation at the endothelial cell surface. The blunted response of $Anxa2^{-/-}$ endothelial cells to hypoxia was not because of impairment of the HIF system, because HIF-1α was stabilized equally in $Anxa2^{+/+}$ and $Anxa2^{-/-}$ retinal tissue during OIR and in endothelial cells after exposure to hypoxia (supplemental Figure 5A-B).

Annexin A2 system–mediated proteolysis relieves the fibrin blockade to retinal angiogenesis

When maintained in room air, $Anxa2^{-/-}$ retinas exhibited fibrin that was readily detectable immunologically. $Anxa2^{+/+}$ retinas, however, displayed only trace amounts of detectable fibrin (supplemental Figure 6). During OIR, $Anxa2^{-/-}$ retinas exhibited high levels of perivascular fibrin deposition compared with $Anxa2^{+/+}$ retinas, in which only small amounts of fibrin were identified (Figure 5A-B). When A2 expression was restored in $Anxa2^{-/-}$ on subretinal injection of an A2-encoding adenovirus, fibrin deposition decreased to the level observed in the $Anxa2^{+/+}$ retina (Figure 5C-D).

Furthermore, systemic treatment of mouse pups on release from hyperoxia with the defibrinating agent, ancrod,[23] reduced plasma fibrinogen by > 80% (Figure 6A). This treatment, which eliminated fibrin deposition in both $Anxa2^{-/-}$ and $Anxa2^{+/+}$ retinas (Figure 6B-C; supplemental Figure 7A-C), more than doubled retinal neovascularization in $Anxa2^{-/-}$, but not $Anxa2^{+/+}$, retinas (Figure 6D-E; supplemental Figure 7D-E). Ancrod also nearly

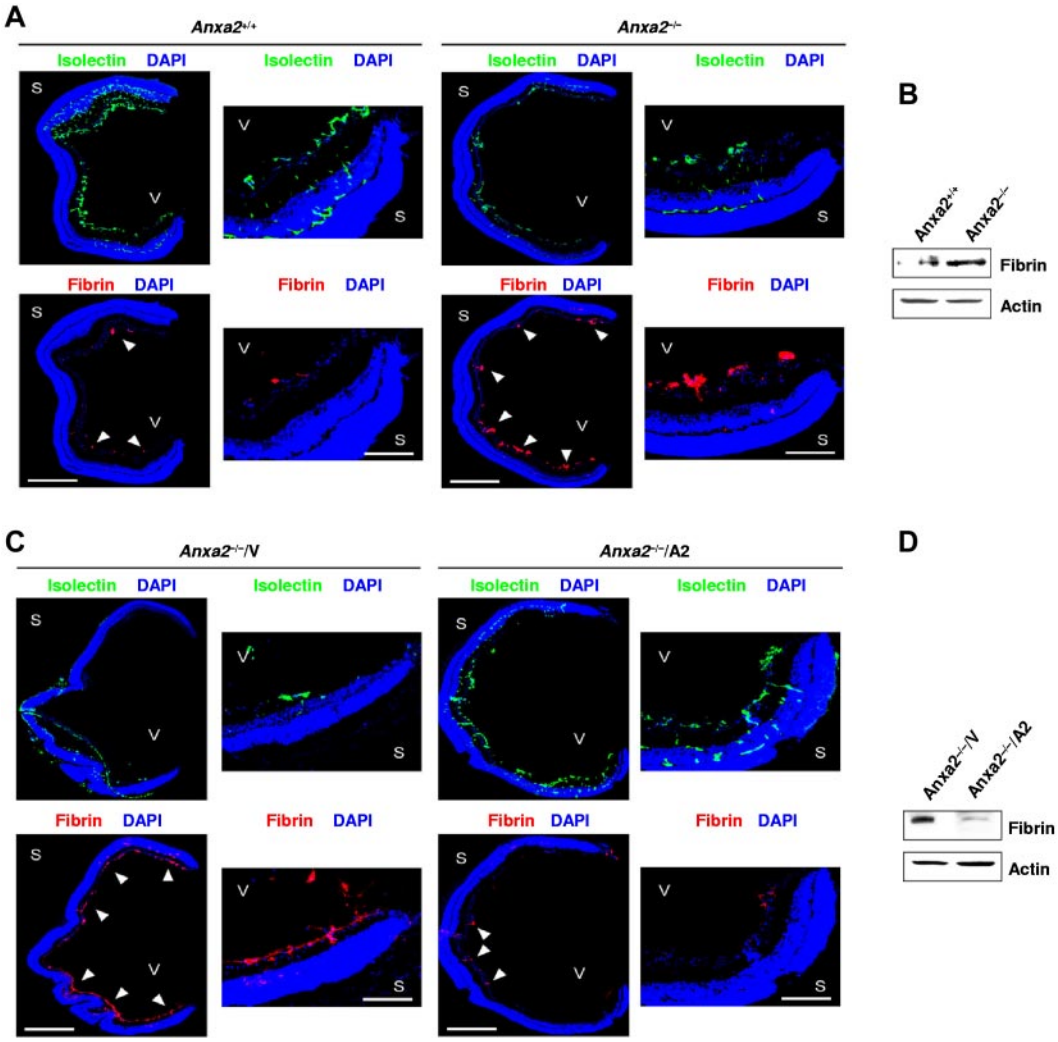

Figure 5. The annexin A2 system promotes retinal neoangiogenesis in OIR by enhancing fibrin clearance. (A) Representative cross-sections (magnification ×40) of retinas, from P17 oxygen-treated *Anxa2*$^{+/+}$ and Anxa2$^{-/-}$ mice, stained with DAPI (blue), isolectin B4 (green), and anti-fibrinogen (red). Close-up views of the peripheral retina are also shown (magnification ×200). Fibrin deposition is indicated by arrowheads. (B) Representative immunoblot of fibrin within retinal tissue from P17 oxygen-treated *Anxa2*$^{+/+}$ and *Anxa2*$^{-/-}$ mice. (C) Representative cross-sections (magnification ×40) of retinas from P17 oxygen-treated *Anxa2*$^{-/-}$ mice injected with either empty (V) or A2-encoding (A2) virus, stained with DAPI (blue), isolectin B4 (green), and anti-fibrinogen (red). Close-up views of the peripheral retina are also shown (magnification ×200). Fibrin deposition is indicated by arrowheads. (D) Representative immunoblot of fibrin within retinal tissue from P17 oxygen-treated *Anxa2*$^{-/-}$ mice injected with empty or A2-encoding virus. S indicates sclera; V, vitreous body. Scale bars, 500 μm (A; magnification ×40) and 100 μm (C; magnification ×200). The data are representative of 5 (A,C) and 3 (B,D) independent experiments.

doubled the number of neovascular tuft nuclei in Anxa2$^{-/-}$ (Figure 6F) but not Anxa2$^{+/+}$ (supplemental Figure 7F) retinas at P17, whereas the retinal vaso-obliteration phase of OIR remained unchanged.

Conversely, we treated mouse pups, immediately on their release from hyperoxia, with tranexamic acid (TA), an inhibitor of plasminogen activation.[24] Under conditions in which systemic TA impaired plasma clot lysis (Figure 7A), fibrin deposition increased dramatically in the retina (Figure 7B-C). At the same time, both retinal neovascularization and neovascular tuft nuclei decreased by more than one-half by P17 (Figure 7D-F). Similar reductions in tPA-dependent clot lysis activity, retinal neoangiogenesis, and neovascular nuclei, accompanied by increases in fibrin deposition, were observed in P17, TA-treated *Anxa2*$^{-/-}$ mice, even though OIR was already depressed (supplemental Figure 8). Together, these data suggest that fibrin is a potent modulator of oxygen-induced retinal neoangiogenesis.

Discussion

Metazoan cells sense tissue oxygen tension through the action of prolyl-4-hydroxylases, which use oxygen as a substrate to hydroxylate and mark HIF-1α for proteasomal destruction.[25] Essentially, all critical angiogenic factors, including secreted VEGF, stromal-derived growth factor, angiopoietin 2, PlGF, platelet-derived growth factor B, stem cell factor, and erythropoietin, as well as many growth factor receptors, signal transduction molecules, and transcription factors are induced by hypoxia, either directly or indirectly, through HIF-1.[25,26] The current study places annexin A2 within this group by presenting the first evidence that the annexin A2 gene is transcriptionally regulated in hypoxia through the direct action of HIF-1.

HIF-1 is a ubiquitous, heterodimeric protein consisting of HIF-1α, which is oxygen regulated, and HIF-1β, which is

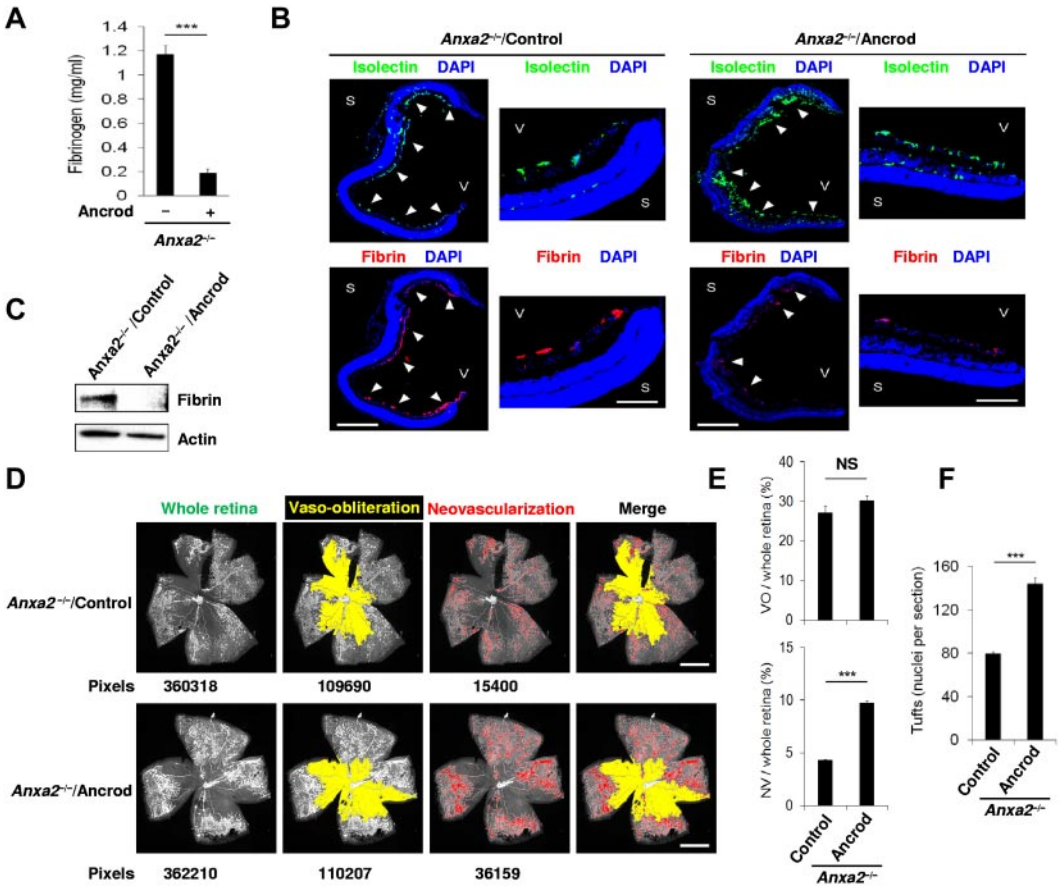

Figure 6. Fibrinogen depletion enables neovascularization of the *Anxa2*$^{-/-}$ retina. (A) ELISA of fibrinogen levels in plasma from P17 Anxa2$^{-/-}$ mice treated with (0.19 ± 0.04 mg/mL; n = 7) or without (1.17 ± 0.09 mg/mL; n = 8) ancrod (***$P < .001$). (B) Representative cross-sections (magnification ×40) of retinas from P17 oxygen-treated *Anxa2*$^{-/-}$ mice treated thereafter with or without ancrod and stained with DAPI (blue), isolectin B4 (green), and anti-fibrinogen (red). Close-up views of the peripheral retina are also shown (magnification ×200). S indicates sclera; V, vitreous body. Scale bars 500 and 100 μm, for magnification ×40 and ×200, respectively. (C) Representative immunoblot of fibrin in retinal tissue from P17 oxygen-treated *Anxa2*$^{-/-}$ mice treated thereafter with or without ancrod. (D) Representative images showing total retinal area and regions of AV and VO from P17 oxygen-treated Anxa2$^{-/-}$ mice treated thereafter with or without ancrod. Pixel number corresponding to each compartment is indicated below each image. Scale bars, 200 μm (magnification ×50). (E) Ratios of areas of VO to total retina (27.2% ± 1.7% vs 30.1% ± 1.3%) and NV to total retina (4.3% ± 0.09% vs 9.7% ± 0.2%) in P17 oxygen-treated *Anxa2*$^{-/-}$ mice treated thereafter with or without ancrod (n = 5; NS indicates no significant difference, *** $P < .001$). (F) Enumeration of neovascular nuclei in retinal sections from P17 oxygen-treated *Anxa2*$^{-/-}$ mice treated thereafter with (131.8 ± 5.3 nuclei per section) or without ancrod (79.4 ± 2.2 nuclei per section; n = 5; ***$P < .001$). The data are representative of 5 (B) or 3 (C) independent experiments.

constitutively expressed.[27] Under normoxic conditions, HIF-1α undergoes hydroxylation at proline 402 or 564 or both, which allows it to bind to the von Hippel-Lindau protein and recruit an E3 ubiquitin ligase. Ubiquitination of HIF-1α results in its degradation in the proteasome.[28,29] Hypoxia inhibits prolyl hydroxylase activity, allowing the intracellular accumulation of HIF-1α, which translocates to the nucleus and dimerizes with HIF-1β. On target genes, the HIF-1α/β complex binds to *cis*-acting HREs, which contain the consensus sequence 5′-(A/G)CGTG-3′.[16]

The OIR model has long been used to study the effects of retinal ischemia on the subsequent angiogenic response. In this respect, it is a robust model of ROP, as well as other retinal vascular proliferative disorders, such as diabetic retinopathy. In both OIR and ROP, high-level oxygen causes regression of developing or newly developed blood vessels (vaso-obliteration), resulting in a zone of ischemia within the central retina. Retinal ischemia leads to rapid up-regulation of HIF-1α, especially within the ganglion cell layer, which houses the retina's vascular plexus.[30,31] HIF-1 then drives transcriptional induction of oxygen-regulated genes.

Our data describe a novel pathway for the regulation of A2 within the hypoxic endothelial cell (supplemental Figure 9). We show that, on stabilization, HIF-1α, presumably in complex with HIF-1β, interacts directly with a putative HRE within the 5′-untranslated region of the A2 gene, leading to activation of the A2 promoter. This interaction resulted in an increase in promoter activity similar to that seen with HIF-α induction of VEGF. Increased transcription of A2 mRNA resulted in higher A2 protein levels and stabilization of p11.[9] Cell surface A2 and p11 also increased in response to hypoxia-induced phosphorylation of pp60src kinase activation[32] and A2 tyrosine phosphorylation[15] and was associated with enhanced plasmin generation and migration through a fibrin barrier. Our previous data have shown that annexin A2 undergoes tyrosine phosphorylation through the action of pp60src kinase, which is activated in response to heat shock, and that this event is required for translocation of A2 to the cell surface.[15] In the present study, we found that activation of src increases dramatically under hypoxia, and, along with increased total expression of both A2 and p11, probably contributes to the enhanced surface expression of both proteins. Plasmin may activate selected matrix metalloproteinases,[33] further facilitating the directed migration of endothelial cells and other vascular cells. Plasmin or matrix metalloproteinases or both may also release extracellular matrix-associated angiogenic growth factors that further support neovascularization of the retina.[34]

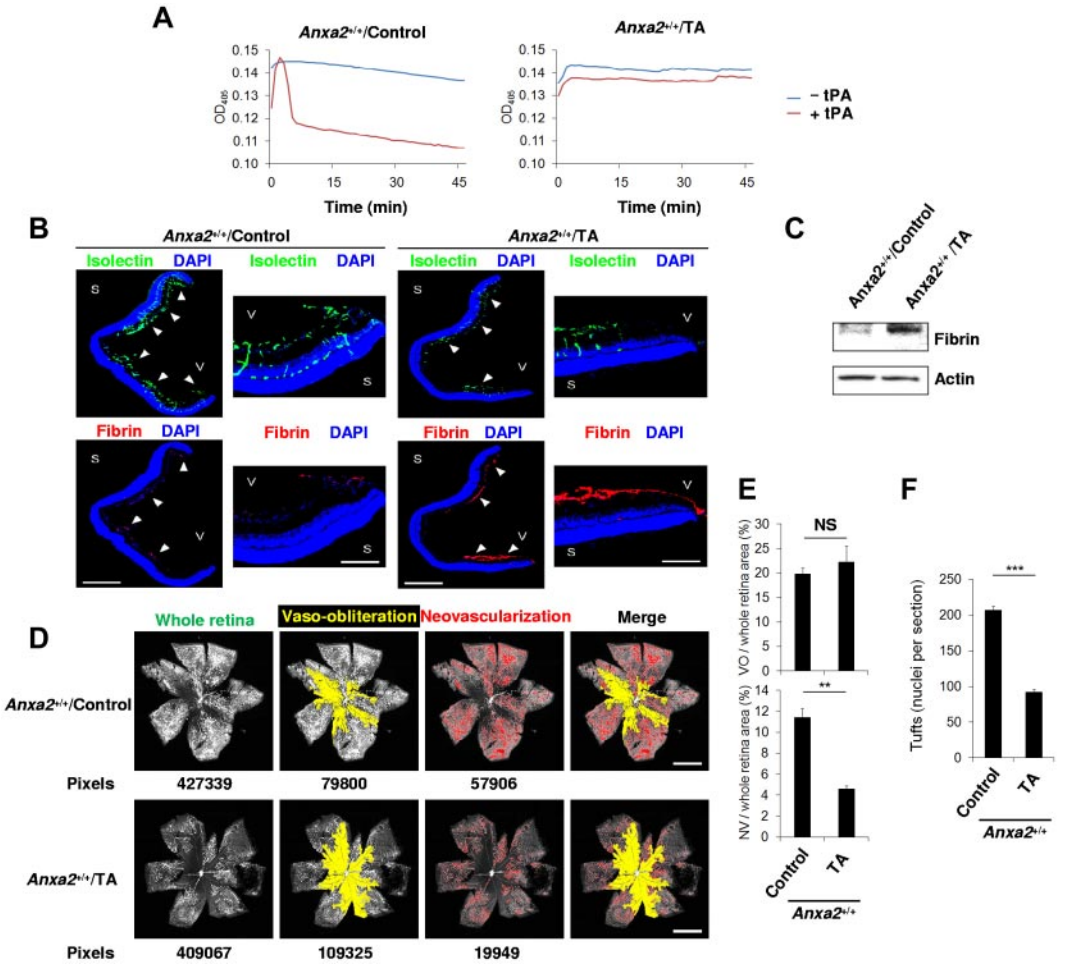

Figure 7. Interruption of fibrinolysis blocks retinal neoangiogenesis during OIR. (A) Clot lysis curves representative of ≥ 3 assays (n = 4 for each) performed with plasma from P17 *Anxa2*$^{+/+}$ mice treated with or without TA. (B) Representative cross-sections (magnification ×40) of retinas from P17 oxygen-treated *Anxa2*$^{+/+}$ mice treated with or without TA and stained with DAPI (blue), isolectin B4 (green), and anti-fibrinogen (red). Close-up views of the peripheral retina (magnification ×200) are also shown. Fibrin deposition is indicated by arrowheads. S indicates sclera; V, vitreous body. Scale bars 500 and 100 μm for magnification ×40 and ×200, respectively. (C) Representative immunoblot of fibrin in retinas from P17 oxygen-treated Anxa2$^{+/+}$ mice treated with or without TA. (D) Representative images from P17 oxygen-treated *Anxa2*$^{+/+}$ mice treated with or without TA, showing total retinal area and regions of VO and NV. Pixel number corresponding to each compartment is indicated below each image. Scale bars, 200 μm (magnification ×50). (E) Ratios of VO to total retinal area (19.8% ± 1.3% vs 22.2% ± 3.3%) and NV to total area (11.4% ± 0.9% vs 4.6% ± 0.3%) in retinas from P17 oxygen-treated *Anxa2*$^{+/+}$ mice treated with or without TA (n = 4; NS indicates no significant difference, ***$P < .001$). (F) Enumeration of neovascular nuclei in retinas from P17 oxygen-treated *Anxa2*$^{+/+}$ mice treated with (92 ± 4.0; n = 5) or without TA (207 ± 5.9; n = 3; ***$P < .001$). The data are representative of 5 (B) or 3 (C) independent experiments.

The present work is also the first, to our knowledge, to identify fibrin and the vascular fibrinolytic system as critical regulators of retinal angiogenesis in vivo. Fibrin deposition was dramatically increased in the posthyperoxic *Anxa2*$^{-/-}$, but not *Anxa2*$^{+/+}$, retina, and prevention of fibrin deposition restored retinal angiogenesis, whereas inhibition of fibrinolysis curtailed it. The precise mechanism by which fibrin may block neoangiogenesis is unclear. Individual degradation products of fibrin and fibrinogen have been reported to stimulate such diverse and even opposing activities as vascular contractility,[35] leukocyte activation and inhibition,[36] endothelial cell proliferation and apoptosis,[37,38] and smooth muscle cell proliferation.[39] In addition, fibrin might constitute a physical barrier to the directed migration of plasmin-deficient endothelial cells or could harbor essential growth factors that are released only on localized proteolysis by plasmin.

The mouse retina has long served as a model for studying both physiologic and pathologic angiogenesis without the need for surgical manipulation of tissues.[40] Indeed, the importance of a number of pathways involving VEGF, erythropoietin, insulin-like growth factor, BM progenitor cells, and lipid-derived mediators of angiogenesis have emerged from work that was based on the mouse OIR model. Although OIR, as a model of human retinal proliferative disease, may be most relevant to retinopathy of prematurity, it also recapitulates several key features of proliferative diabetic retinopathy. These include the development of pathologic neovessels in response to earlier vessel loss,[41] loss of integrity of the blood-retinal barrier with vascular leak,[42] and concomitant glial and neuronal damage in association with retinal vascular disease.[43] Therefore, our findings in the *Anxa2*$^{-/-}$ mouse may have implications that extend beyond ROP to diabetic retinopathy or possibly age-related macular degeneration.

For high-risk ROP, laser ablative therapy and, more recently, anti-VEGF modalities are the mainstays of treatment.[44] Left untreated, unfavorable outcomes in ROP may be as high as 56%.[45] Even with laser therapy, undesirable visual and structural sequelae may be seen in 10%-15% of treated patients,[46] some of whom progress to retinal detachment.[47] Although anti-VEGF–based treatments to prevent or reverse ROP are encouraging, further randomized control trials are needed to assess dosage regimens and potential late neurologic and ocular complications.[48] Clinical trials

to evaluate treatment with insulin-like growth factor-1 were recently initiated, and dietary supplementation of ω-3 polyunsaturated fatty acids may also be tested as a preventative measure in the near future.[47]

Our results suggest a potential new therapeutic target for ROP and possibly other proliferative retinopathies. Although systemic antifibrinolytic therapy with tranexamic acid, aprotinin, or ϵ aminocaproic acid has been used to treat fibrinolysis in association with dental procedures, major surgery, menorrhagia, and traumatic hyphema,[24] enthusiasm for its systemic use has been dampened by reports of seizure activity, myocardial infarction, and stroke in adults[49,50] and aortic thrombosis in a child.[51] The stressed premature newborn, moreover, may have exaggerated fibrinolytic activity, with elevated levels of tPA, urokinase, or both,[52,53] whose activity might be overcome only with large doses of antifibrinolytics, thus increasing the likelihood of untoward effects, such as thrombosis. Therefore, local, intraocular blockade of the annexin A2 system might provide a safer alternative by attenuating cell surface fibrinolysis, specifically in the perivascular compartment, and without disrupting systemic hemostatic balance. Indeed, a recent study suggests that chlorotoxin, an agent that interacts with annexin A2, may prevent or reverse ocular neovascularization in several mouse models.[54]

Acknowledgments

The authors thank C. Greenberg and J. Rivera (Weill Cornell Medical College) for technical assistance, G. Semenza (Johns Hopkins University) for providing Hif1a$^{+/+}$ and Hif1a$^{-/-}$ MEFs and the pBluescript/HIF1A vector, O. Hankinson (University of California, Los Angeles) for providing the pBM5/HIF1B expression vector, B. Vogelstein (Johns Hopkins University) for providing pAdTrack-CMV and pAdEasy-1 vectors, and L. Ellis (M. D. Anderson Cancer Center) for providing the VEGF luciferase reporter vector.

This work was supported by the NIH (grants HL 042493, HL 090895, and HL 046403, K.A.H.) and the March of Dimes (grant 6-FY05-94, K.A.H.).

Authorship

Contribution: B.H. designed and conducted the experiments, analyzed the data, and prepared the manuscript; A.B.D. conducted experiments and analyzed the data; K.-L.H. conducted experiments; K.C. conducted experiments and analyzed the data; G.S., D.A., P.H., and P.B. assisted with the experiments; A.T.J. provided unpublished promoter sequence data; and K.A.H. supervised the study, analyzed the data, and revised the manuscript.

Conflict-of-interest disclosure: The authors declare no competing financial interests.

The current affiliation for K.L.H. is Division of Hematology, Department of Internal Medicine, Ninth People's Hospital Affiliate, Jiao Tong University School of Medicine, Shanghai, People's Republic of China. The current affiliation for G.S. is Division of Endocrinology, Department of Medicine, Albert Einstein College of Medicine, Bronx, NY.

Correspondence: Katherine A. Hajjar, Department of Cell and Developmental Biology, Weill Cornell Medical College 1300 York Ave, Box 45, New York, NY 10065; e-mail: khajjar@med.cornell.edu.

References

1. Chen J, Smith LEH. Retinopathy of prematurity. *Angiogenesis.* 2007;10(2):133-140.
2. Sapieha P, Joyal JS, Rivera JC, et al. Retinopathy of prematurity: Understanding ischemic retinal vasculopathies at an extreme of life. *J Clin Invest.* 2010;120(9):3022-3032.
3. Gerke V, Creutz CE, Moss SE. Annexins: Linking Ca++ signalling to membrane dynamics. *Nat Rev Mol Cell Biol.* 2005;6(6):449-461.
4. Dassah M, Deora A, He K, Hajjar KA. The endothelial cell annexin A2 system and vascular fibrinolysis. *Gen Physiol Biophys.* 2009;28:F20-F28.
5. Kwon M, MacLeod TJ, Zhang Y, Waisman DM. S100A10, annexin A2, and annexin A2 heterotetramer as candidate plasmnogen receptors. *Front Biosci.* 2005;10:300-325.
6. Hajjar KA, Jacovina AT, Chacko J. An endothelial cell receptor for plasminogen/tissue plasminogen activator: I. Identity with annexin II. *J Biol Chem.* 1994;269(33):21191-21197.
7. Cesarman GM, Guevara CA, Hajjar KA. An endothelial cell receptor for plasminogen/tissue plasminogen activator. II: annexin II-mediated enhancement of t-PA-dependent plasminogen activation. *J Biol Chem.* 1994;269(33):21198-21203.
8. O'Connell PA, Surette AP, Liwski RS, Svenningsson P, Waisman DM. S100A10 regulates plasminogen-dependent macrophage invasion. *Blood.* 2010; 116(7):1136-1146.
9. He K, Deora AB, Xiong H, et al. Endothelial cell annexin A2 regulates polyubiquitination and degradation of its binding partner, S100A10/p11. *J Biol Chem.* 2008;283(28):19192-19200.
10. Ling Q, Jacovina AT, Deora AB, et al. Annexin II is a key regulator of fibrin homeostasis and neoangiogenesis. *J Clin Invest.* 2004;113(1):38-48.
11. Jacovina AT, Deora AB, Ling Q, et al. Homocysteine inhibits neoangiogenesis in mice through blockade of annexin A2-dependent fibrinolysis. *J Clin Invest.* 2009;119(11):3384-3394.
12. Smith LE, Wesolowski E, McLellan A, et al. Oxygen-induced retinopathy in the mouse. *Invest Ophthalmol Vis Sci.* 1994;35(1):101-111.
13. Chen J, Connor KM, Aderman CM, Smith LEH. Erythropoietin deficiency decreases vascular stability in mice. *J Clin Invest.* 2008;118(2):526-533.
14. Connor KM, Krah NM, Dennison RJ, et al. Quantification of oxygen-induced retinopathy in the mouse: A model of vessel loss, vessel regrowth and pathological abgiogenesis *Nat Protocols.* 2009;4(11):1565-1573.
15. Deora AB, Kreitzer G, Jacovina AT, Hajjar KA. An annexin 2 phosphorylation switch mediates its p11-dependent translocation to the cell surface. *J Biol Chem.* 2004;279(42):43411-43418.
16. Fukuda R, Zhang H, Kim J, Shimoda L, Dang CV, Semenza GL. HIF-1 regulates cytochrome oxidase subunits to optimize efficiency of respiration in hypoxic cells. *Cell.* 2007;129(1):111-122.
17. He T, Zhou S, Da Costa LT, Yu J, Kinzler KW, Vogelstein B. A simplified system for generating recombinant adenoviruses. *Proc Natl Acad Sci U S A.* 1998;95(5):2509-2514.
18. Cesarman-Maus G, Rios-Luna NP, Deora AB, et al. Autoantibodies against the fibrinolytic receptor, annexin 2, in antiphospholipid syndrome. *Blood.* 2006;107(11):4375-4382.
19. Kren BT, Steer CJ. Posttranscriptional regulation of gene expression in liver regeneration: role of mRNA stability. *FASEB J.* 1996;10(5):559-573.
20. Forsythe JA, Jiang BH, Iyer NV, et al. Activation of vascular endothelial growth factor gene transcription by hypoxia-inducible factor 1. *Mol Cell Biol.* 1996;16(9):4604-4613.
21. Chachami G, Simos G, Hatziefthimiou A, Bonanou S, Molyvdas P, Paraskeva E. Cobalt induces hypoxia-inducible factor-1alpha expression in airway smooth muscle cells by a reactive oxygen species- and PI3K-dependent mechanism. *Am J Respir Cell Mol Biol.* 2004;31(5):544-551.
22. Berra E, Benizri E, Ginouves A, Volmat V, Roux D, Pouyssegur J. HIF prolyl-hydroxylase 2 is a key oxygen sensor setting low steady-state levels of HIF-1alpha in normoxia. *EMBO J.* 2003; 22(6):4082-4090.
23. Pizzo SV, Schwartz ML, Hill RL, McKee PA. Mechanism of ancrod anticoagulation. A direct proteolytic effect on fibrin. *J Clin Invest.* 1972; 51(11):2841-2859.
24. Dunn CJ, Goa KL. Tranexamic acid: a review of its use in surgery and other indications. *Drugs.* 1999;57(6):1005-1032.
25. Rey S, Semenza GL. Hypoxia-inducible factor-1-dependent mechanisms of vascularization and vascular remodeling. *Cardiovasc Res.* 2010; 86(2):236-242.
26. Manalo DJ, Rowan A, Lavoie T, et al. Transcriptional regulation of vascular endothelial cell responses to hypoxia by HIF-1. *Blood.* 2005;105(2): 659-669.
27. Wang GL, Jiang BH, Rue EA, Semenza GL. Hypoxia-inducible factor 1 is a basic-helix-loop-helix-PAS heterodimer regulated by cellular O2 tension. *Proc Natl Acad Sci U S A.* 1995;92(12): 5510-5514.
28. Maxwell PH, Wiesener MS, Chang GW, et al. The tumor suppressor protein VHL targets hypoxia-inducible factors for oxygen-dependent proteolysis. *Nature.* 1999;399(6733):271-275.

29. Jaakkola P, Mole DR, Tian YM, et al. Targeting of HIF-1alpha to the von Hippel-Lindau ubiquitylation complex by O2-regulated prolyl hydroxylation. *Science.* 2001;292(5516):468-472.

30. Ozaki H, Yu AY, Della N, et al. Hypoxia inducible factor-1alpha is increased in ischemic retina: Temporal and spatial correlation with VEGF expression. *Invest Ophthalmol Vis Sci.* 1999;40(1): 182-189.

31. Mowat FM, Luhmann UFO, Smith AJ, et al. HIF-1alpha and HIF-2alpha are differentially activated in distinct cell populations in retinal ischaemia. *PLoS One.* 2010;5(6):e11103-e11112.

32. Mukhopadhyay D, Tsiokas L, Zhou XM, Foster D, Brugger JS, Sukhatme VP. Hypoxic induction of human vascular endothelial growth factor expression through c-Src activation. *Nature.* 1995; 375(6532):577-581.

33. Loskutoff DJ, Quigley JP. PAI-1, fibrosis, and the elusive provisional fibrin matrix. *J Clin Invest.* 2000;106(12):1441-1443.

34. Falcone DJ, McCaffrey TA, Haimovitz-Friedman A, Vergilio JA, Nicholson AC. Macrophage and foam cell release of matrix-bound growth factors. Role of plasminogen activation. *J Biol Chem.* 1993;268(16): 11951-11958.

35. Buluk K, Malofiegen M. The pharmacologic properties of fibrinogen degradation products. *Br J Pharmacol.* 1969;35(1):79-89.

36. Richardson DL, Pepper DS, Kay AB. Chemotaxis for human monocytes by fibrinogen degradation products. *Br J Haematol.* 1976;32(4):507-513.

37. Bootle-Wilbraham CA, Tazzyman S, Thompson WD, Stirk CM, Lewis CE. Fibrin fragment E stimulates the proliferation, migration, and differentiation of human microvascular endothelial cells in vitro. *Angiogenesis.* 2001;4(4):269-275.

38. Guo YH, Hernandez I, Isermann B, et al. Caveolin-1-dependent apoptosis induced by fibrin degradation products. *Blood.* 2009;113(18):4431-4439.

39. Naito M, Stirk CM, Smith EB, Thompson WD. Smooth muscle cell outgrowth stimulated by fibrin degradation products. *Thromb Res.* 2000;98(2): 165-174.

40. Stahl A, Connor KM, Sapieha P, et al. The mouse retina as an angiogenesis model. *Invest Ophthalmol Vis Sci.* 2010;51(6):2813-2826.

41. Hardy P, Beauchamp M, Sennlaub F, et al. New insights into the retinal circulation: Inflammatory lipid mediators in ischemic retinopathy. *Prostaglandins Leukot Essent Fatty Acids.* 2005;72(5): 301-325.

42. Zhang SX, Ma JX, Sima J, et al. Genetic differences in susceptibility to the blood-retina barrier breakdown in diabetes and oxygen-induced retinopathy. *Am J Pathol.* 2005;166(1):313-321.

43. Fletcher EL, Downie LE, Hatzopoulos K, et al. The significance of neuronal and glial cell changes in the rat retina during oxygen-induced retinopathy. *Doc Ophthalmol.* 2010;120(1):67-86.

44. Mintz-Hittner HA, Kennedy KA, Chuang AZ. Efficacy of intravitreal bevacizumab for stage 3+ retinopathy of prematurity. *N Engl J Med.* 2011; 364(7):603-615.

45. Multicenter trial of cryotherapy for retinopathy of prematurity. *Arch Ophthalmol.* 1990;108(10): 1408-1416.

46. Good WV. Final results of the early treatment for retinopathy of prematurity (ETROP) randomized trial. *Trans Am Ophthalmol Soc.* 2004;102:233-250.

47. Mantagos IS, Vanderveen DK, Smith LEH. Emerging treatments for retinopathy of prematurity. *Sem Ophthalmol.* 2009;24(2):82-86.

48. Micieli JA, Surkont M, Smith AF. A systematic analysis of the off-label use of bevacizumab for severe retinopathy of prematurity. *Am J Ophthalmol.* 2009;148:536-543.

49. Sander M, Spies CD, Martiny V, Rosenthal C, Wernecke KD. Mortality associated with administration of high-dose tranexamic acid and aprotinin in primary open-heart procedures: A retrospective analysis. *Critical Care.* 2010;14(4):R148-R162.

50. Mangano DT, Tudor IC, Dietzel C. The risk associated with aprotinin in cardiac surgery. *N Engl J Med.* 2006;354(4):353-365.

51. Hocker JR, Saving KL. Fatal aortic thrombosis in a neonate during infusion of epsilon-aminocaproic acid. *J Ped Surgery.* 1995;30(10):1490-1492.

52. Albisetti M. The fibrinolytic system in children. *Sem Thromb Haemost.* 2009;29:339-347.

53. Kingsmore SF, Kennedy N, Halliday HL, et al. Identification of diagnostic biomarkers for infection in premature infants. *Mol Cell Proteomics.* 2008;7(10):1863-1875.

54. Lima e Silva R, Shen J, Gong YY, et al. Agents that bind annexin A2 suppress ocular neovascularization. *J Cell Physiol.* 2010;225(3):855-864.